Korpi, Antti; Kostiainen, Mauri A.

Sol-Gel Synthesis of Mesoporous Silica Using a Protein Crystal Template

Published in:
ChemNanoMat

DOI:
10.1002/cnma.202100458

Published: 01/04/2022

Document Version
Publisher's PDF, also known as Version of record

ACES Asian Chemical Editorial Society

doi.org/10.1002/cnma.202100458

CHEMNANOMAT
Research Article

www.chemnanomat.org

Sol-Gel Synthesis of Mesoporous Silica Using a Protein Crystal Template

Antti Korpi and Mauri A. Kostiainen*[a]

Abstract: Mesoporous materials are useful for a wide range of applications, but control over the dimensions of the porous structure in this size regime remains challenging. Protein cages possess regular shape and many of them fall into the mesoporous size-region, making them potential template materials for inorganic matrices. Here, apoferritin single crystals are used as templates for the production of mesoporous silica. The high free volume and large pore size of the crystals enable silica precursor hydrolysis and condensation inside them and thus templated growth of a silica matrix. Apoferritin can be removed by calcination to yield solid state structures with the crystalline periodicity retained in the mesopores. We foresee that the method is applicable also for other protein cages, enabling production of mesoporous silica with various pore dimensions.

Introduction

Control over molecular structure in nanoscale is of major importance when designing new functional materials. Besides distribution of matter, voids in structures also contribute to functionality of a material, as they are pathways for small molecules to pass through. Porous materials contain empty spaces throughout them, providing a high surface area. This makes them applicable as, for example, adsorbents[1,2] and catalysts,[3] as well as potential materials in biomedicine, most notably as drug delivery agents.[4–6] Porous structures are classified by the pore size: micro- (less than 2 nm), meso- (2–50 nm) and microporous (larger than 50 nm).[7] Permeability of the materials often increases with the expense of mechanical properties as the proportion of voids in the material increases, and appropriate size can be selected according to application.[8] Mesoporous materials are fascinating, as the pore size allows low molecular weight species to pass through, while retaining multimolecular assemblies. Such structures have been confirmed applicable to drug delivery[9] and catalysis.[10]

Numerous template-free methods exist for the production of mesoporous structures, but they are often experimentally complicated or the obtained pores are heterogeneous.[11] These problems can be overcome by using template methods, where a mold is used to cast a matrix material and later removed. If a well-defined template is used, the pores can also be uniform in both size and three-dimensional (3D) orientation relative to each other. Biomolecules are promising templates, as their structures can often be precisely controlled in nanoscale[12] and even in situ.[13] Biomolecules also enable production of more complex templates than most synthetic molecules due to their specific shapes and surface properties.[14,15] Self-assembly of, for example, proteins can yield scaffolds with specific nanoscale structures and macroscale shapes.[16] Furthermore, using organic templates and inorganic matrices is a straightforward method for carrying out the process, as organic molecules can be removed by calcination, yielding a porous inorganic material.[17] However, preparing porous materials this way, especially in the pore size regime of 10–30 nm, is often challenging due to the lack of suitable templates. Furthermore, template materials can be difficult to arrange in a well-defined manner, leading to poor spatial orientation and wide size distribution of the pores.[7]

Protein cages are relatively large protein nanoparticles characterized by a hollow interior. Compared to many other molecular species, self-assembly of protein cages is an especially interesting phenomenon, as the particles are already in the size range of 10–50 nm in diameter, yet rigid and uniform in shape and size.[18] The cages also possess site specific functionalities and can assemble in a controlled manner.[19–21] Therefore, protein cages can form highly porous crystals with macroscopic dimensions.[22,23] Consequently, protein cage assemblies are versatile scaffold materials[24,25] and promising templates for mesoporous materials.

Silica gel is a suitable matrix material for crystals as it can be synthesized in mild conditions where proteins can retain their shape and functionality.[26] Silica is also a commonly used material in biomedicine due to its robustness and biocompatibility[27] and it has been used in protein-based template systems, enabling facile separation by calcination and production of hierarchical porous materials.[28,29] Additionally, depending on the method of preparing the silica gel, it can provide protein crystals with additional stability and be used to affect the morphology of the crystals.[30]

In this study, we use ferritin crystals as templates to produce mesoporous silica, as presented schematically in Figure 1.

[a] A. Korpi, Prof. M. A. Kostiainen
Department of Bioproducts and Biosystems
Aalto University
FI-00076 Aalto (Finland)
E-mail: mauri.kostiainen@aalto.fi

Supporting information for this article is available on the WWW under https://doi.org/10.1002/cnma.202100458

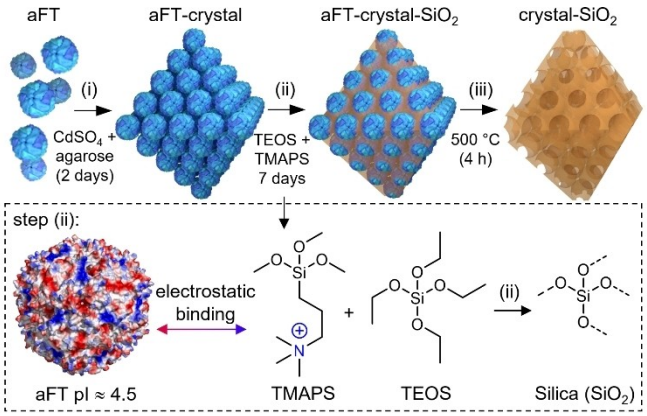

Figure 1. Schematic representation of the production of mesoporous silica. aFT cages (i) self-assemble into crystals with $CdSO_4$ released from agarose gel. (ii) The crystals are mixed with pre-hydrolysed cationic clusters composed of TMAPS and TEOS, which bind to aFT by electrostatic attraction. The clusters condense into silica that encases the crystals (aFT-crystal-SiO_2). (iii) aFT is removed by calcination to obtain mesoporous silica (crystal-SiO_2).

Empty ferritin cages, referred to as apoferritin (aFT), were used as the protein units. aFT is a spherical protein cage with an outer diameter of 12 nm and an inner cavity of 8 nm and its native function is to store and release iron. aFT dimensions fall in the mesoporous size region and it has been studied as a template for functional materials due to its encapsulation capabilities.[31,32]

We have previously shown that aFT can be assembled into crystalline lattices by electrostatic self-assembly with various cationic particles. The size of these intermediary particles determines the dimensions of the crystals, including the spacing of individual ferritin cages in them.[33–36] In this study we aimed to produce large single crystals with high free volume and used metal cations to promote the crystallization. Thus, the spacing arising from other factors than aFT cages themselves is suppressed. Encasing the crystals in inorganic material enables embedding of the same ordered structure into the matrix, which is then isolated by removing the proteins.

Results and Discussion

Crystallization of aFT was carried out using the hanging drop vapor diffusion (HDVD) method.[37] In this technique, crystallization is promoted by gradual increase in reagent concentration due to evaporation of solvent. Such slow crystal formation favors large well-defined assemblies. $CdSO_4$ was used as a co-crystallization agent to initiate the electrostatic self-assembly between the anionic aFT cages and cationic Cd^{2+} ions. Additionally, $CdSO_4$ was first immobilized in agarose gel and placed in contact with the aFT solution. The setup creates a high concentration gradient to the interface between the gel and the protein solution, promoting crystallization at these points.[38] This leads to the formation of fewer crystals with larger individual size. $(NH_4)_2SO_4$ was also included in the crystallization solution to further promote crystal growth, as it has been reported to enhance protein precipitation from aqueous solutions.[39] The complete crystallization procedure is described in Supporting Information Section 1. Optical microscopy (OM) and scanning electron microscopy (SEM) show octahedral crystals with dimensions as large as 100 μm (Figure 2a and 2b, respectively). Octahedral crystals are typical for both body centred cubic (BCC) and face centred cubic (FCC) structures composed of spherical particles, as crystallization proceeds symmetrically outwards from the nucleus and is fastest along [111] direction, yielding particles defined by eight [111] planes as faces.[40]

In small angle X-ray scattering (SAXS) analysis, nine intensity maxima can be clearly observed from the crystals (Figure 2c). They are identified as Bragg reflections from (111), (200), (220), (311), (400), (420) and (442) and are found at relative positions $q/q^* = \sqrt{3}$, 2, $\sqrt{8}$, $\sqrt{11}$, 4, $\sqrt{20}$, $\sqrt{24}$, $\sqrt{27}$ and 6, respectively. These peaks correspond with allowed reflections from an FCC crystal. Lattice constant (a) of the structure is calculated by plotting the quadric Miller indices against the measured q values and defining slope of linear fit of the data points (Figure 2d), yielding $\sqrt{(h^2+k^2+l^2)} = 29.16\ q$ (Å^{-1}), and a is obtained using equation $a = (2\pi\sqrt{(h^2+k^2+l^2)})/q_{hkl} = 18.3$ nm. The centre-to-centre distance (d_{cc}) between neighboring aFT cages is $d_{cc} = a/\sqrt{2} = 13.0$ nm. Such compact structure is to be expected as the co-assembly agent is a simple ion and much smaller than aFT, so it does not contribute significantly to the dimensions of the structures. FCC is a structure that has been

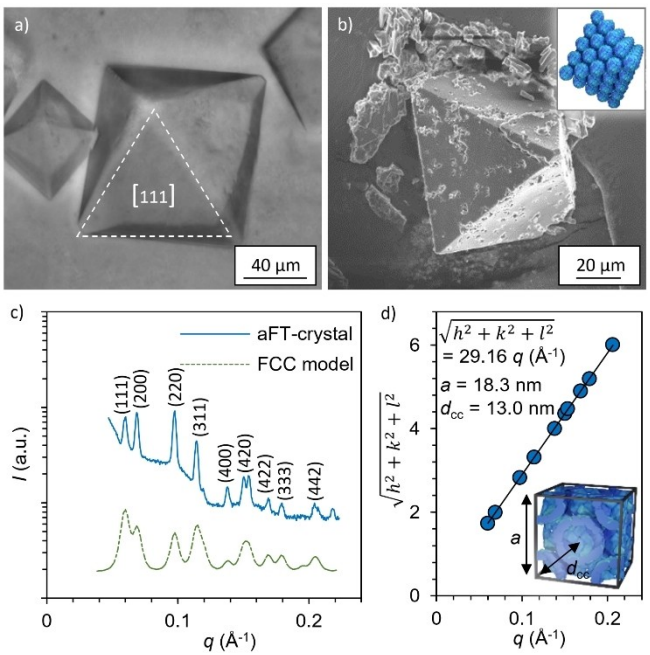

Figure 2. Structure of the aFT crystals. a) OM and b) SEM images show the octahedral habit of the crystals with large smooth surfaces that can cover several μm^2. c) SAXS analysis shows that the crystals have an FCC structure, where several scattering maxima can be identified. d) Linear fit of the quadric Miller indices of assigned reflections for $Fm\bar{3}m$ structure as a function of the measured q-vector positions from aFT crystals. Slope of the fit is used to determine unit cell dimensions $a = 18.3$ nm and $d_{cc} = 13.0$ nm.

also previously reported for electrostatically self-assembled aFT systems.[34,36]

The obtained crystals were first cross-linked with glutaraldehyde and then encased in inorganic matrix by mixing them with tetraethoxysilane (TEOS) and N-[3-(trimethoxysilyl]propyl)-N,N,N-trimethylammonium chloride (TMAPS), that condense into silica gel through a sol-gel reaction. TEOS and TMAPS were pre-hydrolyzed to create small cationic clusters, which can adhere on the anionic aFT surface and promote silica deposition. Such step has been found crucial in, for example, production of DNA nanostructure directed silica composites.[41] Finally, the crystals were suspended into the silica solution for seven days. OM and SEM imaging of the silica encased crystals show that the crystals stay intact during the process and retain their octahedral shape (Figure 3a–b). Furthermore, formation of silica takes place primarily in conjunction with the crystals instead of unspecific clustering and deposition, which enables them to stay separated during the sol-gel reaction. Silica coating can also be seen on the surface of crystals using SEM. SAXS analysis of the aFT-crystal-SiO_2 confirms that the crystal structure is retained inside the silica (Figure 3e). FCC structure with the same dimensions as the aFT crystals can be observed (see Supporting Information Figure S3a).

To obtain porous structures, aFT-crystal-SiO_2 samples were calcinated at 500 °C for 4 hours. SAXS shows that the crystalline periodicity templated by aFT persists in silica after calcination with only a small change in the spacing between the pores compared to that of aFT in the crystals (Figure 3e). Similar calculations that were conducted for pre-calcinated materials reveal that silica has FCC structure with $a = 18.0$ nm and $d_{cc} = 12.7$ nm (see Supporting Information Figure S3b), indicating a slight structure compaction due to silica dehydration during calcination.[42] Structure compaction and slightly different contrast result to small changes in the scattering pattern, such as less intense (311) peak, as would be expected for such changes. However, as the peaks can be identified even at high q-values, the pores appear to be still well ordered. The size change is only 2% compared to the original aFT crystals, proving that silica is largely unaffected by the process and therefore houses the porous structure (Figure 3e inset). OM imaging supports this finding as the calcinated silica retains the shape of the crystals and they appear denser and slightly compacted (Figure 3c). SEM shows more clearly that the structure of aFT crystals has been transferred into silica, as the octahedral 3D shape can be observed, especially in the case of small crystals (Figure 3d). However, silica is not uniform on the surface of the

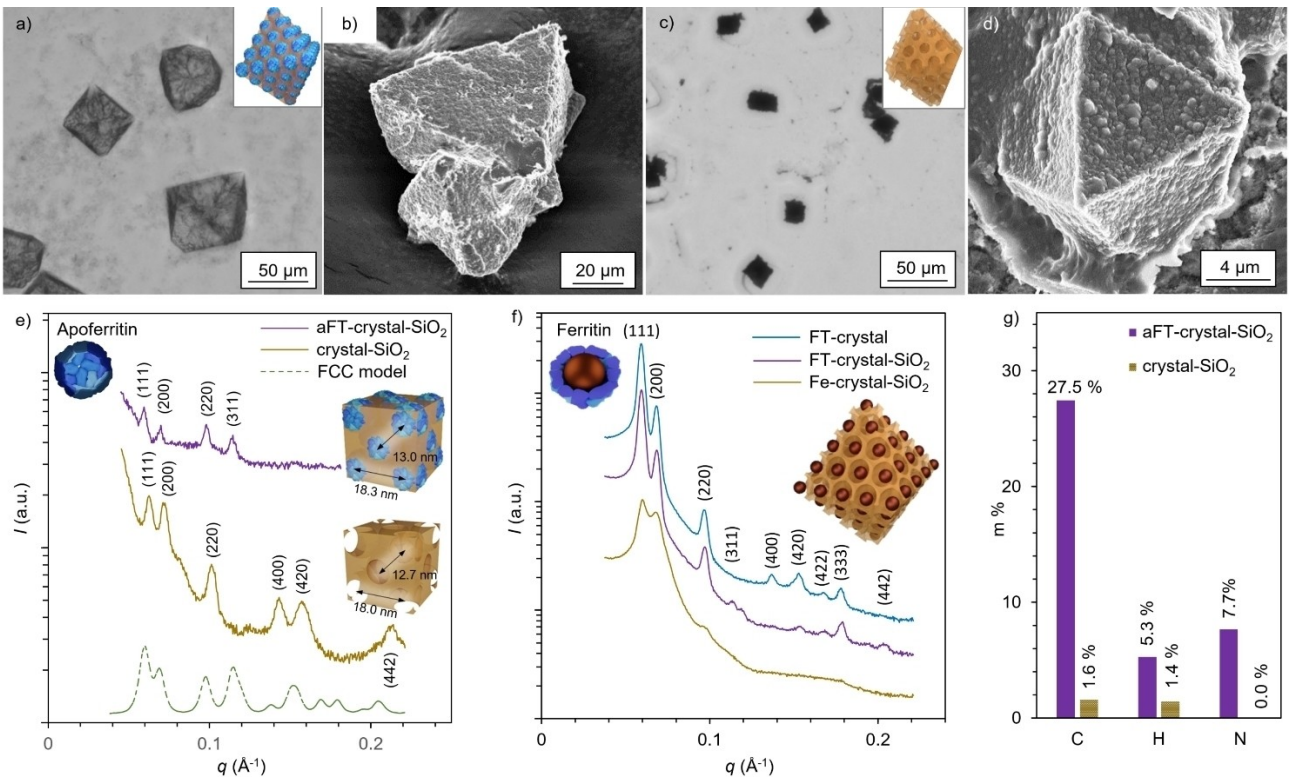

Figure 3. The effects of silica encapsulation and calcination on aFT crystals. a) OM and b) SEM imaging of the silica encased aFT crystals show that the crystal habit is retained during the silica deposition. c) OM and d) SEM imaging of the calcinated crystals confirms that the octahedral habit is largely retained also after removal of aFT. e) SAXS measurements of the silica material before and after calcination confirm that aFT retains its FCC crystal structure during the encasing and the same structure largely remains after calcination. Insets: Schematic representations of silica embedded aFT crystal and calcinated silica showing the lattice parameters and centre-to-centre distance. f) SAXS measurements of the materials prepared using iron-containing FT as template. The FT containing samples had the same FCC structures and dimensions as the samples prepared using aFT, but in the calcinated sample the scattering pattern is less clear. Inset shows a schematic presentation of the final structure where each cavity holds the residual iron core of FT. g) Elemental analysis confirms the removal of aFT during calcination and shows that the organic material (C, H, N) mass percentage is reduced from 40% to only 3% after the heat treatment.

particles, as uneven patterns can be observed both before and after calcination. This is probably because silica lacs directing support from aFT at the surfaces of the crystals.

Additionally, the possibility of using the protein cage to incorporate additional materials into the mesoporous silica was studied by using crystals composed of ferritin (FT) carrying iron hydroxide nanoparticles instead of aFT as templates. Like silica, inorganic nanoparticles can withstand the calcination process and remain in the final material. The process was studied using SAXS similarly to the aFT samples (Figure 3f). FT crystals (FT-crystal) had the same FCC structure with the $a = 18.3$ nm as the aFT crystals and the nanoparticles scattered X-rays strongly, resulting in clear scattering pattern. As with the aFT samples, the crystal structure remained intact through the silica encasing (FT-crystal-SiO_2), but in the calcinated samples (Fe-crystal-SiO_2) the scattering pattern broadened. The dimensions of the calcinated structure were calculated to be $a = 19.1$ nm and $d_{cc} = 13.5$ nm. Slight increase in the lattice constant and broadening of the intensity maxima is expected as the protein cages no longer hold the nanoparticles in place. However, three scattering maxima can be identified, which match with the FCC model, suggesting that the structure persists. We foresee that similar materials could be produced using other types of metal nanoparticles that can be contained inside ferritin or possibly other protein cages.[43,44]

Recent work with DNA-directed nanoparticle lattices[42] suggests that the spatial order of the aFT and FT templated silica pores could possibly be improved by producing less dense crystal structures. Using co-assembly agents with larger dimensions, for example cationic dendrimers,[34] could enable the pre-hydrolyzed silica to spread though the crystals more easily.

To ensure that protein does not remain embedded inside silica, crystal-SiO_2 combustion was followed using elemental analysis to determine elemental composition of the materials before and after calcination (Figure 3g). Mass of C, H and N constitutes to roughly 40% of the mass of in the pre-calcinated aFT-crystal-SiO_2 sample and is reduced to 3% during calcination, suggesting effective removal of all organic material. Notably, N is removed completely, indicating that no protein is left after calcination, as mass of proteins, including aFT, arises mostly from C and N. Silica cannot be detected in the analysis but contributes to the overall mass of the sample.

The produced mesoporous silica structures can supposedly hold small molecules or particles inside the pores and provide sustained release. To test these properties, doxorubicin (dox) was adsorbed to the calcinated silica and released in dialysis. The amount of the released dox was followed using UV-vis spectrometer. For comparison, the process was repeated using silica material prepared without aFT crystals and therefore without the mesoporous structure. The release of known amount of dox through a dialysis membrane was also followed (Figure 4a). Silica was able to adsorb approximately 10% of its own mass of dox and gradually release it in a period of up to 24 hours, demonstrating the possibility of using crystal-SiO_2 as a sustained release agent. However, silica without the mesoporous structure has also a sufficient surface area, enabling it to interact with dox in a similar manner. Therefore, the current

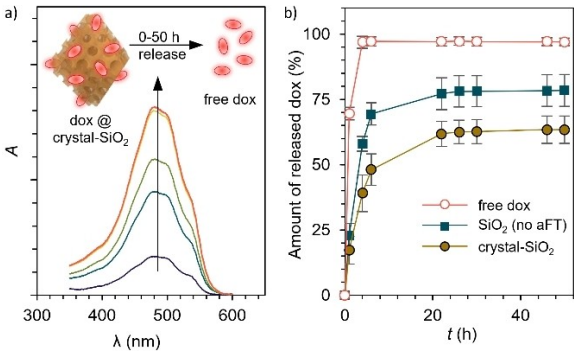

Figure 4. Dox release experiments. Silica prepared in presence and absence of aFT crystals were loaded with dox. a) Release from crystal-SiO_2 observed using UV-vis spectroscopy. b) Kinetic plots for release from different silica materials. The release was completed in 24 hours and the mesoporous material detained dox slightly better.

mesoporous structure does not greatly enhance these loading properties as all the pores are most likely not fully accessible. The mesoporous silica was slightly more efficient in detaining the dox in time periods of below 20 hours. All the adsorbed dox was not released in the dialysis, as some of it was lost when the solid silica samples were rinsed with a buffer solution before placing them in the dialysis container to avoid moving solution of free dox along with the loaded material. UV-Vis absorbance spectra are shown in the Supporting Information Section 5.

Conclusion

We have developed a method for the preparation of micrometer-scale aFT crystals, which can be encased in silica matrix under neutral conditions. The protein template can be removed by calcination to obtain mesoporous silica material with crystalline periodicity. Besides ferritin, we foresee that the method is also applicable for other protein cages, enabling production of varying porous structures in the future. As protein cages can carry inorganic molecules inside them, the cargo molecules could also be incorporated into the silica matrix. Such ordered and fixed active sites can be useful in catalysis and biomedical applications once the pore accessibility is optimized.[45,46]

Experimental Section

Materials

All the reagents were used as received without further purification. Apoferritin (aFT) from *Pyrococcus furiosus* was provided by MoLiRom, agarose by Biotop and $(NH_4)_2SO_4$ by Fluka Analytical. Tetraethoxysilane (TEOS), glutaraldehyde (50% weight ratio in water) and Trizma base for tris buffer were provided by Sigma Aldrich. $CdSO_4$ and N-[3-(trimethoxysilyl)propyl]-N,N,N-trimethylammonium chloride (TMAPS, 50% in methanol) were provided by Alfa Aesar. All the used water was Milli-Q purified.

Sol-gel synthesis of silica

Silica encasing procedure of the aFT crystals was adapted from a previously reported method.[47] Pre-hydrolysed nanoclusters were prepared from tetraethoxysilane (TEOS) and N-[3-(trimethoxysilyl)propyl]-N,N,N-trimethylammonium chloride (TMAPS). 20 µl of TMAPS (50% weight ratio in methanol) was added into 1 ml of 50 mM tris buffer (pH 7.5) under vigorous stirring and let mix for 20 minutes. Then, 20 µl of TEOS was added in small portions under vigorous stirring and let mix for 20 minutes. The resulting solution was clear and homogeneous.

The crosslinked aFT crystals were reacted with a freshly prepared cluster solution by hanging the crystals in the solution in a similar container where the crystallization was carried out. But here, 1 ml of the cluster solution was placed instead of the reservoir solution so that the hanging crystals made contact with the solution. The crystals were left in the solution for 7 days while standing still to ensure even encasing. After this, the crystals were rinsed with water to remove the excess clusters.

For comparison, the silica encasing was also carried out using only TEOS, excluding the charged silica groups from TMAPS. In this experiment, the pre-hydrolysis solution was prepared by adding 40 µl of TEOS into 1 ml of 50 mM tris buffer (pH 7.5) in small portions under vigorous stirring. After an hour of mixing the solution was heterogeneous and was further mixed for another hour in bath sonication at 50 °C, after which the solution was homogeneous. The rest of the procedure was identical to when TEOS and TMAPS was used. Without TMAPS, the silica growth was still focused on the aFT crystals but continued well beyond the crystals (Figure S2), which would supposedly lead to smaller proportion of mesoporous regions in the final silica material.

Silica calcination

The samples were calcinated at 500 °C while open to atmosphere to remove aFT crystals. The temperature was ramped from room temperature to 500 °C over 2 hours, kept at 500 °C for 4 hours and ramped back to room temperature over 2 hours. The samples were calcinated on top of the glass slides they were crystallized on.

Optical microscopy

Optical microscopy imaging was carried out using Zeiss Axio Vert A1 inverted microscope. Samples were imaged on top of the same glass slides which were used for the crystallization process without further preparation.

Scanning electron microscopy

Scanning electron microscopy (SEM) imaging was carried out using Zeiss Sigma VP SEM. Accelerating voltage was 8.00 kV and InLens detector was used for all acquisitions. Samples were transferred onto aluminium stubs using conductive two-sided graphene tape. The tape was placed onto a sample dried in air, removed and placed onto the sample stub with the sample side up. Prior to SEM imaging, the samples were sputtered with 1 nm layer of Ir using Leica EM AC600 sputtering device.

Small angle X-ray scattering

Small angle X-ray scattering (SAXS) analysis was carried out using Xenocs Xeuss 3.0 instrument. Cu Kα radiation (λ = 1.54 Å) was used as the direct beam with collimation set for standard flux and sample to detector distance was 800 mm. Detector distance was calibrated using silver behenate standard. The entire instrument, including the sample and the detector, were in vacuum during the scattering measurements.

One-dimensional (1D) SAXS data were obtained by azimuthally averaging the recorded 2D scattering patterns. Magnitude of the scattering vector q is given by equation $q = \frac{4\pi \sin\theta}{\lambda}$, where 2θ is the scattering angle. The data were analysed using Scatter software version 2.5. For the Si treated aFT samples presented in Figure 3, a power law background $I(q) = Bq^{-P}$, where $P = 1.62$ was subtracted from the data. Data without any background subtraction is presented in Figure S3.

SAXS samples were prepared by placing the sample inside a steel washer sealed from both sides with Kapton film. The film isolates the sample from the vacuum of the instrument and does not have scattering peaks in the observed q-range. 10 µl of undiluted solutions were used as liquid samples and roughly 3 mg of powder as solid samples.

Elemental analysis

The elemental analysis of silica before and after calcination was carried out using Thermo Scientific FlashSmart EA CHNS/O instrument operated at 1000 °C. Silica encased aFT crystals were dried under N_2 flow at room temperature prior to the analysis. For the elemental analysis, approximately 1.5 mg of each dry sample was weighed into a Sn cup an analysed.

UV-vis spectroscopy

Adsorption of doxorubicin (dox) into calcinated silica samples was studied using UV-vis spectroscopy by adaptation of a previously reported method.[48] The experiment was carried out with mesoporous silica prepared using aFT crystal template and plain silica material, which was prepared in a similar manner, except that no aFT crystals were present. 1 mg of dry silica was placed in 1 ml of 2 mg/ml dox solution in an Eppendorf tube that was placed in shaker overnight. The samples were centrifuged and supernatant removed. The samples were washed with 500 µl of 40 mM tris buffer (pH 7.5), samples centrifuged, supernatant removed and washing was repeated. The samples were placed in dialysis cups (MWCO 20 kDa) and dialysed against 18 ml of water. After 1, 4, 6, 22, 26, 30, 46 and 50 hours of dialysis 1 ml of dialysis solutions were collected and their absorption spectrum was recorded between 350 and 600 nm (Figure S4). To determine the dox concentration, absorption at 495 nm was selected as an observation point as it is an absorption maximum for dox. Each sample was returned to the dialysis solution after the analysis. The measurements were performed in duplicate.

To determine the amount of dox adsorbed by the samples, the absorption spectra of the original supernatant was compared with that of 2 mg/ml dox solution. The absorption at 495 nm showed that 1 mg of aFT-templated silica adsorbed 0.13 mg of dox and control silica 0.12 mg. In repeated experiments aFT-templated silica adsorber 0.11 mg of dox and control silica 0.12 mg. For comparison, release of free dox in dialysis was studied in a similar manner by loading 0.12 mg of dox in 1 ml of 40 mM tris buffer (pH 7.5) against 17 ml of water.

Acknowledgements

This work has received funding from the European Research Council (ERC) under the European Union's Horizon 2020 research and innovation programme (Grant agreement No. 101002258). We acknowledge the provision of facilities at OtaNano – Nanomicroscopy Center (Aalto-NMC) and Bioeconomy Infrastructure. Funding from Academy of Finland (projects 308578, 303804, 267497), the Jane and Aatos Erkko Foundation, Aalto University School of Chemical Engineering and Finnish Foundation for Technology Promotion are acknowledged.

Conflict of Interest

The authors declare no conflict of interest.

Data Availability Statement

The data that support the findings of this study are available from the corresponding author upon reasonable request.

Keywords: Apoferritin · crystal self-assembly · mesoporous silica · protein cages

[1] A. Walcarius, L. Mercier, *J. Mater. Chem.* **2010**, *20*, 4478.
[2] K. Ariga, A. Vinu, Y. Yamauchi, Q. Ji, J. P. Hill, *BCSJ* **2012**, *85*, 1–32.
[3] Y. Lin, J. Ren, X. Qu, *Acc. Chem. Res.* **2014**, *47*, 1097–1105.
[4] M. Vallet-Regí, F. Balas, D. Arcos, *Angew. Chem. Int. Ed.* **2007**, *46*, 7548–7558; *Angew. Chem.* **2007**, *119*, 7692–7703.
[5] I. Slowing, J. Viveroescoto, C. Wu, V. Lin, *Adv. Drug Delivery Rev.* **2008**, *60*, 1278–1288.
[6] F. Tang, L. Li, D. Chen, *Adv. Mater.* **2012**, *24*, 1504–1534.
[7] F. Hoffmann, M. Cornelius, J. Morell, M. Fröba, *Angew. Chem. Int. Ed.* **2006**, *45*, 3216–3251; *Angew. Chem.* **2006**, *118*, 3290–3328.
[8] G. J. de A. A. Soler-Illia, C. Sanchez, B. Lebeau, J. Patarin, *Chem. Rev.* **2002**, *102*, 4093–4138.
[9] Y. Wang, Q. Zhao, N. Han, L. Bai, J. Li, J. Liu, E. Che, L. Hu, Q. Zhang, T. Jiang, S. Wang, *Nanomedicine Nanotechnology, Biol. Med.* **2015**, *11*, 313–327; N. V. Jadhav, P. R. Vavia, *AAPS PharmSciTech* **2017**, *18*, 2764–2773.
[10] Y. Dai, V. Pavan Kumar, C. Zhu, M. J. MacLachlan, K. J. Smith, M. O. Wolf, *ACS Appl. Mater. Interfaces* **2018**, *10*, 477–487.
[11] S. Lehman, S. Larsen, *Environ. Sci.-Nano* **2014**, *1*, 200–213; S. Ahoulou, N. Vilà, S. Pillet, D. Schaniel, A. Walcarius, *Chem. Mater.* **2019**, *31*, 5796–5807.
[12] T. K. Nguyen, H. Negishi, S. Abe, T. Ueno, *Chem. Sci.* **2019**, *10*, 1046–1051.
[13] R. Alberstein, Y. Suzuki, F. Paesani, F. A. Tezcan, *Nat. Chem.* **2018**, *10*, 732–739.
[14] J. C. Falkner, M. E. Turner, J. K. Bosworth, T. J. Trentler, J. E. Johnson, T. Lin, V. L. Colvin, *J. Am. Chem. Soc.* **2005**, *127*, 5274–5275.
[15] Q. Lei, J. Guo, F. Kong, J. Cao, L. Wang, W. Zhu, C. J. Brinker, *J. Am. Chem. Soc.* **2021**, https://doi.org/10.1021/jacs.1c00814.
[16] C. Y. Khripin, D. Pristinski, D. R. Dunphy, C. J. Brinker, B. Kaehr, *ACS Nano* **2011**, *5*, 1401–1409.
[17] M. Antonietti, B. Berton, C. Göltner, H.-P. Hentze, *Adv. Mater.* **1998**, *10*, 154–159.
[18] M. Lach, M. Künzle, T. Beck, *Chem. Eur. J.* **2017**, *23*, 17482–17486.
[19] M.-C. Daniel, I. B. Tsvetkova, Z. T. Quinkert, A. Murali, M. De, V. M. Rotello, C. C. Kao, B. Dragnea, *ACS Nano* **2010**, *4*, 3853–3860.
[20] T. Beck, S. Tetter, M. Künzle, D. Hilvert, *Angew. Chem. Int. Ed.* **2015**, *54*, 937–940; *Angew. Chem.* **2015**, *127*, 951–954.
[21] N. E. Brunk, M. Uchida, B. Lee, M. Fukuto, L. Yang, T. Douglas, V. Jadhao, *ACS Appl. Bio Mater.* **2019**, *2*, 2192–2201.
[22] S. Zhang, *Nat. Biotechnol.* **2003**, *21*, 1171–1178.
[23] A. Korpi, E. Anaya-Plaza, S. Välimäki, M. Kostiainen, *WIREs Nanomed Nanobiotechnol* **2019**, https://doi.org/10.1002/wnan.1578.
[24] M. Künzle, M. Lach, T. Beck, *Dalton Trans.* **2018**, *47*, 10382–10387.
[25] T. K. Nguyen, T. Toan Pham, T. Ueno, *Jpn. J. Appl. Phys.* **2019**, *58*, SI0802.
[26] L. Ellerby, C. Nishida, F. Nishida, S. Yamanaka, B. Dunn, J. Valentine, J. Zink, *Science* **1992**, *255*, 1113–1115.
[27] Z. Li, Y. Zhang, N. Feng, *Expert Opin. Drug Delivery* **2019**, *16*, 219–237.
[28] J. E. Meegan, A. Aggeli, N. Boden, R. Brydson, A. P. Brown, L. Carrick, A. R. Brough, A. Hussain, R. J. Ansell, *Adv. Funct. Mater.* **2004**, *14*, 31–37.
[29] D. Eglin, G. Mosser, M.-M. Giraud-Guille, J. Livage, T. Coradin, *Soft Matter* **2005**, *1*, 129.
[30] J. A. Gavira, A. E. S. Van Driessche, J.-M. Garcia-Ruiz, *Cryst. Growth Des.* **2013**, *13*, 2522–2529; J. A. Gavira, M. Conejero-Muriel, J. M. Delgado-López, *Acta Crystallogr.* **2018**, *D74*, 1200–1207.
[31] S. Fujikawa, E. Muto, T. Kunitake, *Langmuir* **2007**, *23*, 4629–4633.
[32] L. Zhang, J. B. Bailey, R. H. Subramanian, A. Groisman, F. A. Tezcan, *Nature* **2018**, *557*, 86–91.
[33] M. A. Kostiainen, P. Hiekkataipale, A. Laiho, V. Lemieux, J. Seitsonen, J. Ruokolainen, P. Ceci, *Nat. Nanotechnol.* **2013**, *8*, 52–56.
[34] V. Liljeström, J. Seitsonen, M. A. Kostiainen, *ACS Nano* **2015**, *9*, 11278–11285.
[35] J. Mikkilä, E. Anaya-Plaza, V. Liljeström, J. R. Caston, T. Torres, A. de la Escosura, M. A. Kostiainen, *ACS Nano* **2016**, *10*, 1565–1571.
[36] N. K. Beyeh, Nonappa, V. Liljeström, J. Mikkilä, A. Korpi, D. Bochicchio, G. M. Pavan, O. Ikkala, R. H. A. Ras, M. A. Kostiainen, *ACS Nano* **2018**, *12*, 8029–8036.
[37] A. Blackburn, S. Partowmah, H. Brennan, K. Mestizo, C. Stivala, J. Petreczky, A. Perez, A. Horn, S. McSweeney, A. Soares, *Crystals* **2018**, *8*, 464.
[38] F. Artusio, A. Castellví, A. Sacristán, R. Pisano, J. A. Gavira, *Cryst. Growth Des.* **2020**, *20*, 5564–5571.
[39] L. Jiang, L. He, M. Fountoulakis, *J. Chromatogr. A* **2004**, *1023*, 317–320.
[40] S. Tang, Z. Wang, Y. Guo, J. Wang, Y. Yu, Y. Zhou, *Acta Mater.* **2012**, *60*, 5501–5507.
[41] X. Jing, F. Zhang, M. Pan, X. Dai, J. Li, L. Wang, X. Liu, H. Yan, C. Fan, *Nat. Protoc.* **2019**, *14*, 2416–2436.
[42] P. W. Majewski, A. Michelson, M. A. L. Cordeiro, C. Tian, C. Ma, K. Kisslinger, Y. Tian, W. Liu, E. A. Stach, K. G. Yager, O. Gang, *Sci. Adv.* **2021**, *7*, eabf0617.
[43] J. M. Slocik, R. R. Naik, M. O. Stone, D. W. Wright, *J. Mater. Chem.* **2005**, *15*, 749.
[44] M. Künzle, T. Eckert, T. Beck, *J. Am. Chem. Soc.* **2016**, *138*, 12731–12734.
[45] J.-G. Li, C.-Y. Tsai, S.-W. Kuo, *RSC Adv.* **2015**, *5*, 42798–42807.
[46] K. V. Manukyan, A. V. Yeghishyan, C. E. Shuck, D. O. Moskovskikh, S. Rouvimov, E. E. Wolf, A. S. Mukasyan, *Microporous Mesoporous Mater.* **2018**, *257*, 175–184.
[47] X. Jing, F. Zhang, M. Pan, X. Dai, J. Li, L. Wang, X. Liu, H. Yan, C. Fan, *Nat. Protoc.* **2019**, *14*, 2416–2436.
[48] J. Shen, Q. He, Y. Gao, J. Shi, Y. Li, *Nanoscale* **2011**, *3*, 4314–4322.

Manuscript received: November 15, 2021
Revised manuscript received: December 13, 2021
Accepted manuscript online: December 17, 2021
Version of record online: ■■, ■■■

RESEARCH ARTICLE

Apoferritin single crystals are used as a template to prepare oriented and ordered mesoporous silica structures. Condensation of pre-hydrolyzed silica precursors takes place within the crystal voids, transferring the hierarchical structure to the silica. A porous framework is created after protein removal by calcination, which provides high control over the spatial orientation of the structure and size of individual pores.

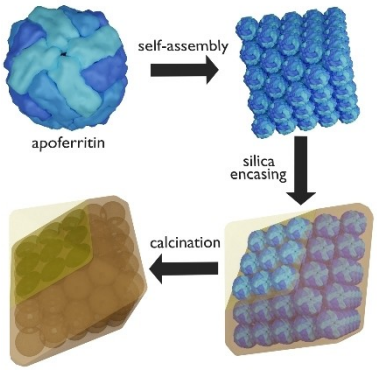

*A. Korpi, Prof. M. A. Kostiainen**